Nuclear Medicine and Biology 96–97 (2021) 41–49

Contents lists available at ScienceDirect

Nuclear Medicine and Biology

journal homepage: www.elsevier.com/locate/nucmedbio

Evaluation of the high affinity [^{18}F]fluoropyridine-candesartan in rats for PET imaging of renal AT_1 receptors

Aida M. Abreu Diaz [a,b,c,d], Gergana O. Drumeva [a,b], Philippe Laporte [c,e], Luis M. Alonso Martinez [a,b,c], Daniil R. Petrenyov [a], Jean-François Carrier [a,c,e,f], Jean N. DaSilva [a,b,c,f,*]

[a] Centre de recherche du Centre hospitalier de l'Université de Montréal, Montréal, Québec, Canada
[b] Département de pharmacologie et physiologie, Faculté de médecine, Université de Montréal, Montréal, Québec, Canada
[c] Institute de génie biomédical, Faculté de médecine, Université de Montréal, Montréal, Québec, Canada
[d] Departamento de Radioquímica, Instituto Superior de Tecnologías y Ciencias Aplicadas, Universidad de la Habana, La Habana, Cuba
[e] Département de physique, Faculté des arts et des sciences, Université de Montréal, Montréal, Québec, Canada
[f] Département de radiologie, radio-oncologie et médecine nucléaire, Faculté de médecine, Université de Montréal, Montréal, Québec, Canada

ARTICLE INFO

Article history:
Received 20 January 2021
Received in revised form 1 March 2021
Accepted 11 March 2021
Available online xxxx

Keywords:
Angiotensin II type 1 receptor
Binding affinity
IC_{50}
Inhibition constant Ki
Radiolabeled metabolites
PET imaging in rats

ABSTRACT

Introduction: Alterations in the expression of the Angiotensin II type 1 receptors (AT_1R) have been demonstrated in the development of several heart and renal diseases. The aim of this study was to evaluate the novel compound [^{18}F]fluoropyridine-candesartan as a PET imaging tracer of AT_1R in rat kidneys.
Methods: Competition binding assays were carried out with membranes from CHO-K1 cells expressing human AT_1R. Binding to plasma proteins was assessed by ultrafiltration. Radiolabeled metabolites in rat plasma and kidneys of control and pretreated animals (candesartan 10 mg/kg or losartan 30 mg/kg) were analyzed by column-switch HPLC. Dynamic PET/CT images of [^{18}F]fluoropyridine-candesartan in male Sprague-Dawley rats were acquired for 60 min at baseline, pre-treatment with the AT_1R antagonist losartan (30 mg/kg) or the AT_2R antagonist PD123,319 (5 mg/kg).
Results: Fluoropyridine-candesartan bound with a high affinity for AT_1R (Ki = 5.9 ± 1.1 nM), comparable to fluoropyridine-losartan but lower than the parent compound candesartan (Ki = 0.4 ± 0.1 nM). [^{18}F] Fluoropyridine-candesartan bound strongly to plasma proteins (99.3%) and was mainly metabolized to radiolabeled hydrophilic compounds, displaying minimal interference on renal AT_1R binding with 82% of unchanged tracer in the kidneys at 20 min post-injection. PET imaging displayed high renal and liver accumulations and slow clearances, with maximum tissue-to-blood ratios of 14 ± 3 and 54 ± 12 in kidney cortex and liver, respectively, at 10 min post-injection. Binding specificity for AT_1R was demonstrated with marked reductions in kidney cortex (−84%) and liver (−93%) tissue-to-blood ratios at 20 min post-injection, when blocking with AT_1R antagonist losartan (30 mg/kg). No change was observed in kidney cortex of rats pre-treated with AT_2R antagonist PD 123,319 (5 mg/kg), confirming binding selectivity for AT_1 over AT_2 receptors.
Conclusion: High kidney-to-blood ratios and binding selectivity to renal AT_1R combined with tracer in vivo stability displaying minimal interference from labeled metabolites support further PET imaging studies with [^{18}F] fluoropyridine-candesartan.

1. Introduction

The renin-angiotensin system (RAS) is recognized as the most powerful hormone system regulating electrolyte balance, body fluid volumes, and blood pressure. In addition to the endocrine system, local RASs exert multiple paracrine/autocrine effects in tissue physiology and homeostasis [1,2]. Angiotensin II (Ang II) is the active peptide responsible for most of the RAS actions in different tissues, mediated mainly through the stimulation of the Ang II type 1 and type 2 receptors (AT_1R and AT_2R, respectively). Alterations in AT_1R levels contribute to several diseases including hypertension, atherosclerosis, heart and renal failure, coronary ischemia, fibrosis, inflammation, cancer and diabetes [3–9]. Treatment of these patients with AT_1R blockers (ARBs) improved clinical outcome [10–13].

Several structural analogs of clinically proven ARBs, such as losartan, irbesartan, valsartan and candesartan, were developed as tracers for positron emission tomography (PET), exhibiting AT_1R-binding specificity in mice, rats, and pigs kidneys [14–23] (Fig. 1, candesartan, losartan and their derived radiotracers). Relevant results were obtained with [^{11}C]KR31173, a derivative of the AT_1R antagonist SK-1080, which showed the feasibility of imaging renal [24–26] and myocardial [27,28] AT_1R in multiple species, including healthy humans [28] and patients with nonobstructive hypertrophic cardiomyopathy [29].

* Corresponding author at: Centre de recherche du Centre hospitalier de l'Université de Montréal, Montréal, Québec, Canada.
E-mail address: jean.dasilva@umontreal.ca (J.N. DaSilva).

https://doi.org/10.1016/j.nucmedbio.2021.03.003
0969-8051/

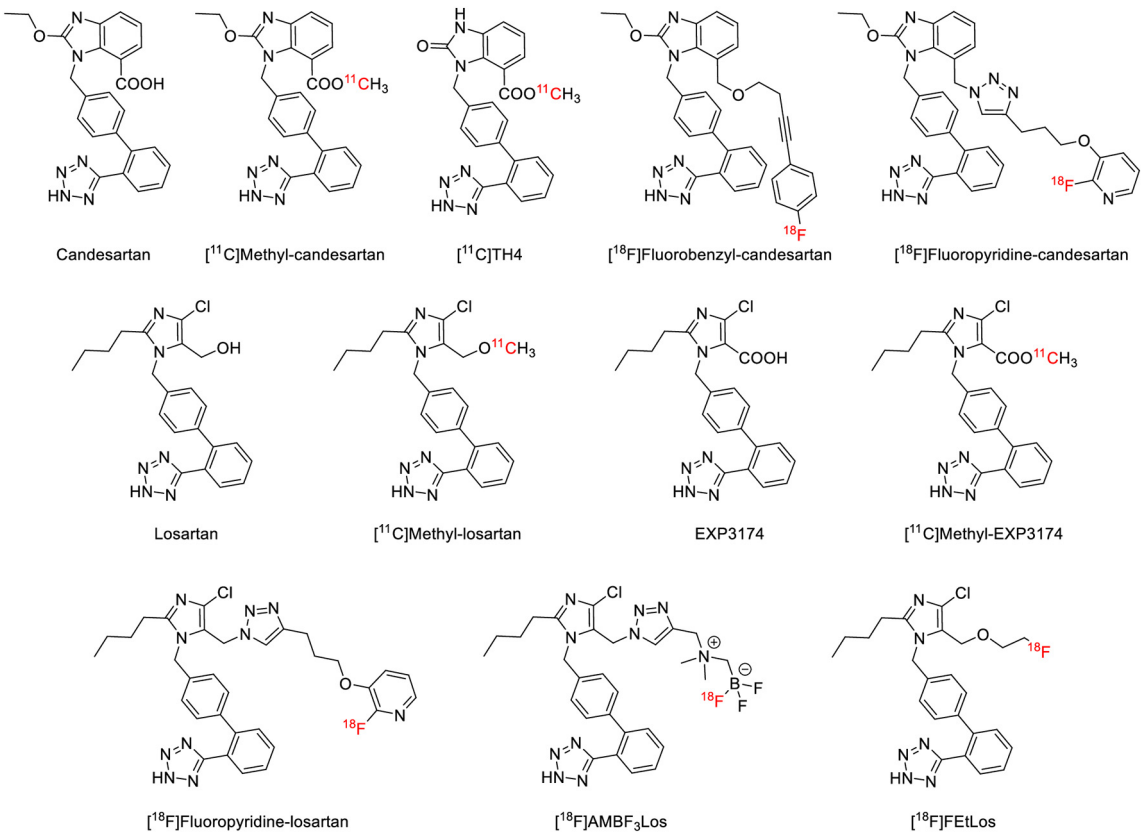

Fig. 1. Chemical structures of candesartan, losartan, EXP3174 (active metabolite of losartan), and their derived radiotracers [14,17–21,33,34].

Candesartan binds to the AT_1R with higher affinity and antagonistic potency (IC_{50} = 0.26 nM) than losartan (IC_{50} = 34 nM). A long-lasting pharmacological effect of candesartan has been associated to a slow dissociation rate from the AT_1R [30–32]. [^{11}C]Methyl-candesartan, developed by our group, exhibited a superior in vivo kinetics and binding profile in rat kidneys [21], compared to [^{11}C]methyl-losartan [19]. However, the labeled hydrophobic metabolite, [^{11}C]TH4 (Fig. 1), exhibited similar binding characteristics as the parent [^{11}C]methyl-candesartan, interfering with the PET signal and thus the AT_1R quantification [21]. On the other hand, the introduction of a [^{18}F]fluoropyridine moiety on the losartan molecule ([^{18}F]fluoropyridine-losartan) produced minimal changes both in binding properties and antagonistic efficacy compared to the parent compound, and little interference of the labeled metabolites on renal AT_1R binding [18]. Using a similar approach, we have synthesized the novel [^{18}F]fluoropyridine analog of the high-affinity candesartan ([^{18}F]fluoropyridine-candesartan) in high purity and molar activity [33]. Biodistribution and autoradiography competition studies in rats confirmed specific binding to renal AT_1R [33] . We also recently developed another ^{18}F-derivative of candesartan ([^{18}F]fluorobenzyl-candesartan) in order to evaluate different structural analogs as potential AT_1R tracers [34]. We hypothesized that [^{18}F] fluoropyridine-candesartan and [^{18}F]fluorobenzyl-candesartan will exhibit high affinity and binding selectivity for AT_1R in PET imaging, and in vivo stability with minimal interference of potential labeled metabolites to renal AT_1R binding in rats.

2. Materials and methods

2.1. Animals

Male Sprague-Dawley rats (168–416 g, Charles River Laboratories, Montreal, Canada) were housed in a temperature-controlled facility on a 12:12 h light/dark cycle and fed standard rat chow and water *ad libitium*. All animal experiments are approved by the Institutional Animal Protection Committees of the Centre de Recherche du Centre Hospitalier de l'Université de Montréal (CRCHUM) and the McGill University Health Centre (MUHC) and conform to the guidelines of the Canadian Council on Animal Care.

2.2. Chemistry and radiochemistry

Commercially available chemicals were used without further purification unless otherwise noted. Fluoropyridine-candesartan, fluorobenzyl-candesartan and fluoropyridine-losartan were synthesized as described previously [17,33,34]. [^{18}F]Fluoropyridine-candesartan was produced with high radiochemical purity (>97%) and molar activity (58–402 GBq/μmol) [33].

2.3. Competition binding assays

Membranes expressing the human AT_1R, prepared from transfected wild-type Chinese hamster ovary cells (CHO-K1) and [^{125}I](Sar^1,Ile^8) Ang II were purchased from PerkinElmer (Waltham, MA, USA). Ang II, candesartan and losartan potassium were obtained from Alomone Labs (Jerusalem, Israel), AstaTech (Bristol, PA, USA) and LKT Laboratories (St Paul, MN, USA), respectively. The binding assays were performed in round bottom 96-well plates (Sarstedt, Montreal, QC, Canada) following previously described procedures [14–16]. In brief, a competitor ligand (Ang II, candesartan, losartan potassium, fluoropyridine-candesartan, fluorobenzyl-candesartan or fluoropyridine-losartan) at increasing final concentrations (10^{-12}–10^{-5} M) in assay buffer (50 mM tris(hydroxymethyl)aminomethane hydrochloride (Tris-HCl), 5 mM $MgCl_2$, pH 7.4) was mixed with [^{125}I](Sar^1,Ile^8)Ang II (final concentration = 0.03 nM) on ice. The AT_1R expressing membranes diluted in assay buffer were added (0.6 μg/well) to a total final volume of 200 μL/well. The plate was covered with a TopSeal-A adhesive film (PerkinElmer, Waltham, MA,

USA) and incubated at room temperature for 60 min with constant shaking (200 rpm). The experiments were terminated by rapid vacuum filtration through Unifilter-96 GF/C filters (PerkinElmer, Waltham, MA, USA) presoaked in blocking buffer (1% Bovine Serum Albumin (BSA) 50 mM Tris-HCl, 5 mM $MgCl_2$, pH 7.4) at 4 °C for 60 min, followed by washing (9 × 250 μL) with ice cold buffer (50 mM Tris-HCl, pH 7.4) using a FilterMate harvester (PerkinElmer, Waltham, MA, USA). Plates were dried and MicroScint-O scintillation cocktail (PerkinElmer, Waltham, MA, USA) was then added (30 μL/well). The luminescence was recorded (3 × 3 min/well) using a TopCount NXT counter (PerkinElmer, Waltham, MA, USA). Nonspecific binding of [^{125}I](Sar^1,Ile^8)Ang II was estimated in the presence of 10^{-5} M unlabeled Ang II and total binding in the absence of competitors. Specific binding was calculated as total binding minus nonspecific binding. The half maximal inhibitory concentration (IC_{50}) values were determined by a four-parameter logistic non-linear regression analysis using GraphPad Prism 8.4.3 software (San Diego, CA, USA). The inhibition constants (Ki) were calculated from the equation $Ki = IC_{50}/(1 + [L] / Kd)$ [16]. Results represent the mean ± standard deviation (SD) of at least three independent experiments performed in single or duplicate (L = [^{125}I](Sar^1,Ile^8)Ang II, [L] = 0.03 nM, and Kd = 0.16 nM). The partition coefficients (cLogP) were predicted using Chem3D Ultra software version 19.1.21 (PerkinElmer, Waltham, MA, USA).

2.4. Plasma-proteins binding

The proportion of [^{18}F]fluoropyridine-candesartan bound to plasma proteins was assessed in three separate experiments (each in triplicate) using the Centrifree Ultrafiltration Device (MWCO = 30,000 Da; Millipore, Oakville, ON, Canada) [18]. The tracer (100 μL) was mixed with 1 mL of pooled plasma and incubated for 5 min at 37 °C. An aliquot of the mix (100 μL) was used as a reference standard. Radioactive plasma (100 μL) was loaded in the upper chamber of the device (n = 3) and centrifuged (2000 ×*g*, 30 min, 4 °C). The resulting filtrate (protein-free fraction) was transferred (60–80 μL) to pre-weighted polypropylene tubes with caps, and counted in a gamma counter (Wizard 3470, PerkinElmer, Waltham, MA, USA). The amount of tracer bound to plasma proteins was calculated as a percentage of the remaining fraction compared to the total activity of unfiltered plasma (based on the radioactive concentration, cpm/g).

2.5. Analysis of radiolabeled metabolites in rats' plasma and kidneys

A modification of the column-switching high-performance liquid chromatography (HPLC) method [35] was used to measure the fractions of unmetabolized [^{18}F]fluoropyridine-candesartan and labeled metabolites in blood plasma and kidney tissue. The system consisted of a capture column: in-line refillable guard column (2 × 20 mm) with 2.5 μm frits (Alltech, ON, Canada) hand-packed with 20 mg of Oasis HLB polymeric reverse phase sorbent (Waters, Milford, MA, USA), 1/99 acetonitrile/water (1 mL/min); switched to an analytical column: Luna C18 10 μm 100 Å 250 × 4.6 mm (Phenomenex, Torrance, CA, USA), 0.1% trifluoroacetic acid in 42/58 acetonitrile/water (2 mL/min) after the elution of biomacromolecules and hydrophilic metabolites (retention time (t_R) of unmetabolized [^{18}F]fluoropyridine-candesartan = 8 min post-switch). The ultraviolet absorbance (254 nm, Waters 2489 detector) and radiation (Raytest Gabi Star detector) were registered with a PeakSimple chromatography data integration system using the PeakSimple software version 4.44 (SRI Instruments, Torrance, CA, USA). Rats received 8–135 MBq of tracer (IV) and were sacrificed at 5 (n = 1), 18 (n = 1), 20 (n = 4), 30 (n = 1), and 60 min (n = 1) post-injection for collection of the trunk blood and removal of the kidneys. The kidneys were analyzed at 20 (n = 4) and 60 min (n = 1) time points. Dissected tissues were homogenized in 80/20 ethanol/water (v/v) using a VWR 200 homogenizer (Radnor, PA, USA) and centrifuged (3000 ×*g*) for 5 min. Supernatant was collected and evaporated, then reconstituted in 200 μL acetonitrile and diluted with 1/99 acetonitrile/water (v/v). Blood was centrifuged (3000 ×*g*) for 5 min to obtain plasma. Urea (0.7 g/mL) was added to disrupt binding to plasma proteins. Before injection into the HPLC system, plasma and kidney extracts were filtered through 0.22 μm syringe filters (Basix, Fisher Scientific, Ottawa, ON, Canada). Similar procedures were followed with three additional groups of rats who received AT_1R antagonists candesartan 10 mg/kg [18,20] (10 mg/mL in 33% sodium bicarbonate (8.4%)/saline (0.9%), IV, n = 4), candesartan 5 mg/kg IV + 5 mg/kg gavage [16] (5 mg/mL in 33% sodium bicarbonate (8.4%)/saline (0.9%), n = 4), or losartan potassium 30 mg/kg [20] (30 mg/mL in saline (0.9%), IV, n = 4), 20 min prior to tracer injection. These rats were sacrificed at 20 min post-injection of [^{18}F]fluoropyridine-candesartan (44–217 MBq, IV). [^{18}F]Fluoropyridine-candesartan formulation was injected into the HPLC to characterize the system and validate the efficiency of the capture cartridge and HPLC system. Frozen samples of rat plasma and kidneys were used as in vitro controls, following incubation with the tracer for 10 min at 37 °C and processing as above, prior to injection into the HPLC system. The data were corrected by radioactive decay and background.

2.6. Small-animals PET/CT imaging

[^{18}F]Fluoropyridine-candesartan (11.00–20.61 MBq, 0.04–0.71 μg non-radioactive mass) microPET/CT scans were acquired in control animals (n = 6) using a Mediso nanoScan PET/CT (Mediso Medical Imaging systems, Budapest, Hungary). To assess binding specificity to AT_1R, an additional group of rats received losartan (30 mg/kg, 30 mg/mL solution as above) 20 min prior to tracer injection (17.97–23.42 MBq, 0.25–0.52 μg non-radioactive mass, n = 3). Another group of rats was injected with the AT_2R antagonist PD 123,319 [17,20] (5 mg/kg, 5 mg/mL in saline 0.9%) 20 min prior to [^{18}F]fluoropyridine-candesartan injection (15.09–24.08 MBq, 0.12–0.35 μg non-radioactive mass, n = 3).

2.6.1. Image acquisition

Small-animal PET/CT studies consisted of a 60 min PET emission scan, followed by a 10 min CT transmission scan for scatter and attenuation correction. Rats were anesthetized throughout the process (induction: 4% isoflurane, 0.5 L/min oxygen; maintenance: <2% isoflurane, 0.5 L/min oxygen) through a nose cone. Animals were placed in a supine position on a heated scanner bed, and the body temperature, respiratory and heart rates were monitored for the duration of the scan, using the Mediso system. Rats were placed in the scanner to include heart and both kidneys in the field of view (FOV). Scans were initiated immediately after the injection of the tracer formulation through the tail vein. A dynamic 60-min scan was acquired as 12 × 10 s, 3 × 60 s, 11 × 300 s frames. MicroPET images were reconstructed using ordered subset expectation maximization (OSEM) algorithm at a voxel size of $(0.4\ mm)^3$, with corrections for scattered and random coincidences, dead time, attenuation, and isotope decay [36].

2.6.2. Image analysis

All images were analyzed with PMOD software version 4.102 (PMOD Technologies, Zurich, Switzerland). Regions of interest (ROIs) were defined on reconstructed images in the left atrium and left kidney cortex to generate time-activity curves, following the procedure previously published [21]. A 3-D sphere was drawn within the left atrium at an early frame (10–30 s) to sample the blood input function. The ROI was defined as the pixels within the sphere corresponding to intensity greater than 80% of the maximal intensity. The kidney ROIs were generated at later frames by drawing a 3-D ellipsoid shape over the two-thirds of the left kidney. The ROI was defined as the pixels inside of the ellipsoid corresponding to intensity greater than 50% of the maximal value within that volume. Furthermore, a 3-D sphere was drawn as an ROI for the liver, over the superior part of the right lobe and at a late frame, usually the same as for the kidney. In that case, all the pixels within the spherical ROI were used. [^{18}F]Fluoropyridine-candesartan renal and hepatic

activities were measured as standardized uptake values normalized to body weight (SUV_{BW}), which allowed relative comparison between subjects. Additionally, kidney-to-blood and liver-to-blood SUV_{BW} ratios were calculated at 5, 10, 20, 30 and 60 min for each scan.

2.7. Statistical analysis

All data are expressed as mean ± SD, as indicated. Two-way ANOVA followed by Tukey's post hoc test to determine source of variability and difference between groups or a two-tailed *t*-test to compare difference between two groups were performed using GraphPad Prism 8.4.3 software for Windows (San Diego, CA, USA). The differences between groups were considered statistically significant when $p < 0.05$.

3. Results

3.1. Competition binding assays

The binding affinities of fluoropyridine-candesartan and fluorobenzyl-candesartan for the human AT_1R expressed in membranes of CHO-K1 cells were evaluated and compared with Ang II, candesartan, losartan potassium and fluoropyridine-losartan (Fig. 2). Fluoropyridine-candesartan exhibited a high binding affinity (Ki = 5.9 ± 1.1 nM, n = 3), similar to fluoropyridine-losartan (Ki = 5.6 ± 2.7 nM, n = 3), and close to their respective parent compounds candesartan (Ki = 0.4 ± 0.1 nM, n = 4) and losartan (Ki = 0.9 ± 0.2 nM, n = 4), as well as Ang II (Ki = 7.3 ± 1.0 nM, n = 3). Surprisingly, fluorobenzyl-candesartan exhibited a 3-orders lower binding affinity (Ki = 1637 ± 653 nM, n = 3) than its lead compound. The rank order of binding affinity for AT_1R was candesartan > losartan > fluoropyridine-candesartan = fluoropyridine-losartan > Ang II > fluorobenzyl-candesartan. Due to the low binding affinity of fluorobenzyl-candesartan for AT_1R, the ^{18}F-analog was not further tested for metabolism or small animal PET.

3.2. Plasma-proteins binding

[^{18}F]Fluoropyridine-candesartan bound to plasma proteins accounted for 99.3 ± 0.2% in plasma (n = 3). No correction was applied to account for plasma-proteins binding when analyzing the PET data.

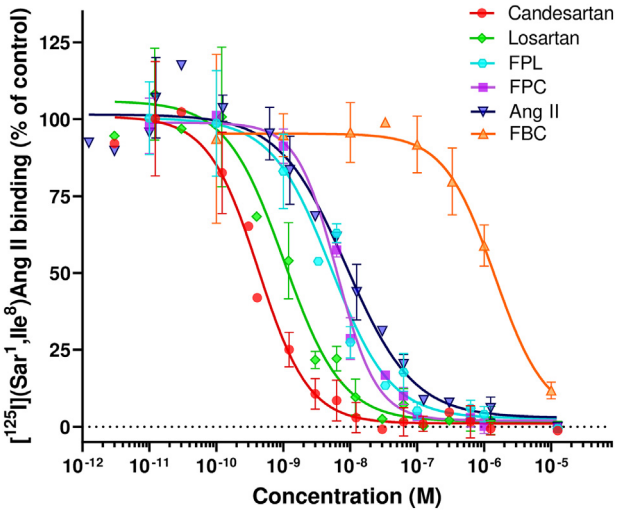

Fig. 2. Competition binding assays of Ang II, candesartan, losartan, fluoropyridine-candesartan (FPC), fluorobenzyl-candesartan (FBC) and fluoropyridine-losartan (FPL) for [^{125}I](Sar^1,Ile^8)Ang II binding to a membrane preparation from CHO-K1 cells expressing the human AT_1R. Data are expressed as a percentage of specific binding in the absence of competitors (% control) and represent the mean ± SD of at least three independent experiments, each performed in single or duplicate.

3.3. Analysis of radiolabeled metabolites in rats' plasma and kidneys

3.3.1. Ex vivo metabolism studies

Radiolabeled metabolite analysis of [^{18}F]fluoropyridine-candesartan revealed three radioactive peaks in control rat plasma at 20 min post-injection, with retention times of approximately 1–2 min after injection (hydrophilic metabolite(s) eluted from the capture column, peak 1), 4 min post-switch (hydrophobic metabolite, peak 2) and 8 min post-switch (unchanged tracer, [^{18}F]FPC) (Fig. 3A). In plasma and kidney in vitro samples spiked with [^{18}F]fluoropyridine-candesartan, the unchanged tracer was present as a major peak (Fig. 3C, D). Ex vivo time-course in plasma samples revealed that the hydrophobic labeled metabolites did not exceed 3% throughout the time of the study (Fig. 4). [^{18}F]Fluoropyridine-candesartan was rapidly washed out from rat plasma, decreasing to 47% at 5 min and remaining around 9% after 30 min, while the hydrophilic metabolites accounted for approximately 90% of the total radioactivity from 30 to 60 min (Fig. 4). As described for plasma, three radioactive peaks were detected in kidney samples at 20 min after injection corresponding to the unchanged tracer ([^{18}F]FPC), hydrophilic (peak 1) and hydrophobic (peak 2) metabolites (Fig. 3B). In kidneys, the proportion of unchanged tracer accounted for 82% at 20 min post-injection and decreased to 42% at 60 min post-injection, while the hydrophilic metabolites increased slowly up to 54% at the last time point. The hydrophobic metabolite fraction had a negligible contribution to the total activity.

3.3.2. Competition studies

At 20 min post-injection, blockade of AT_1R with candesartan (5 mg/kg, IV + 5 mg/kg, gavage) or losartan (30 mg/kg) reduced the unchanged tracer proportion in plasma by 66% ($p < 0.01$) and 51% ($p < 0.05$), respectively (Fig. 5A). At the same time, the fractions of hydrophilic metabolites were increased by 18% ($p < 0.001$) and 14% ($p < 0.01$), respectively (Fig. 5A). No significant differences of proportions in plasma were found in rats pre-treated with candesartan (10 mg/kg) compared to control group. The blocking effects were markedly observed in kidneys with candesartan (10 mg/kg), candesartan (5 mg/kg, IV + 5 mg/kg, gavage), and losartan (30 mg/kg) groups displaying reductions of 57% ($p < 0.0001$), 70% ($p < 0.0001$) and 74% ($p < 0.0001$) of the unchanged tracer compared to control animals, respectively. Meanwhile, the portion of hydrophilic metabolites (peak 1) increased by 4- to 5-fold for the mentioned groups ($p < 0.0001$, Fig. 5B). The fractions of hydrophobic metabolites remained very low in all tested conditions, with no significant changes.

3.4. Small-animals PET/CT imaging

MicroPET images of control untreated rats displayed the highest uptake in the liver and kidney cortex, respectively, with very high contrast with surrounding tissues (Fig. 6A). The time-activity curves exhibited rapid accumulation and slow washout of [^{18}F]fluoropyridine-candesartan in renal cortex and liver, reaching the highest SUV_{BW} at 5 min post-injection, with 4.6 ± 0.8 and 16.1 ± 2.7, respectively (Fig. 6D, E, representative curves). Initial increase in blood activity was observed following injection, which then rapidly decreased back to baseline at 5 min post-injection, allowing for high tissue-to-blood signal contrast from 5 to 30 min and 5–60 min post-injection in kidney cortex and liver, respectively (Fig. 6E).

Pre-treatment with losartan (30 mg/kg) led to a lower kidney and liver signal intensity in PET images (Fig. 6B), inducing 40% ($p < 0.05$) and 69% ($p < 0.0001$) reductions in kidney cortex and liver SUV_{BW} at 20 min post-injection, respectively, in comparison to control group (Figs. 6D, E and 7A, B). Furthermore, a marked decline of the tissue-to-blood ratios was sustained throughout the scanning period for the kidney cortex (e.g. −84% ($p < 0.0001$) at 20 min post-injection, Fig. 7C) and the liver (e.g. −93% ($p < 0.0001$) at 20 min post-injection, Fig. 7D), compared to control group.

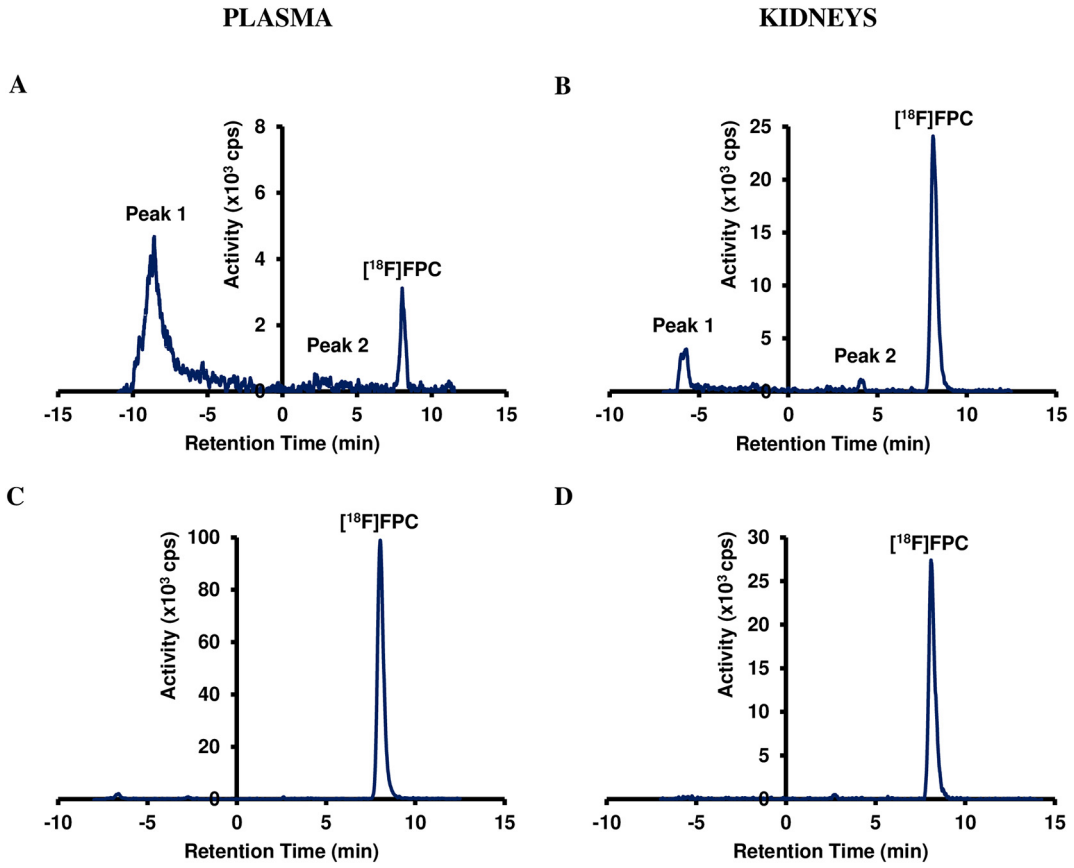

Fig. 3. Representative HPLC chromatograms (decay and background corrected) of radiolabeled metabolites analysis in ex vivo (A) control rats' plasma and (B) kidneys at 20 min after IV injection of [^{18}F]fluoropyridine-candesartan, displaying the presence of unchanged tracer ([^{18}F]FPC) and its labeled metabolites (peaks 1 and 2); and in vitro standards of (C) rat's plasma and (D) kidneys, with one mayor peak corresponding to [^{18}F]fluoropyridine-candesartan. Time = 0 min represents the column switch. [^{18}F]Fluoropyridine-candesartan ([^{18}F]FPC, t_R = 8 min post-switch) is metabolized into hydrophilic metabolite(s) (peak 1, t_R = 1–2 min) and a hydrophobic metabolite (peak 2, t_R = 4 min post-switch).

PET images of rats pre-treated with PD 123,319 exhibited a similar pattern to controls, with high uptake in the rat's liver and kidney cortex (Fig. 6C). No changes in kidney-cortex SUV_{BW} or kidney(cortex)-to-blood ratio were observed over time, in comparison to control group (Figs. 6D and 7A, C). However, administration of the AT_2R inhibitor induced 25% ($p < 0.05$) and 38% ($p < 0.05$) reductions in liver SUV_{BW} and liver-to-blood ratio, respectively, compared to control group at 20 min post-injection, with enhanced effect at the end of the scans (Figs. 6E and 7B, D).

In addition, rats pretreated with losartan displayed reductions in kidney cortex SUV_{BW} (−47%, $p < 0.01$, Fig. 7A), kidney(cortex)-to-blood ratio (−82%, $p < 0.0001$, Fig. 7C), liver SUV_{BW} (−59%, $p < 0.001$, Fig. 7B), and liver-to-blood ratio (−89%, $p < 0.01$, Fig. 7D) when compared to PD 123,319 pre-treated animals at 20 min post-injection.

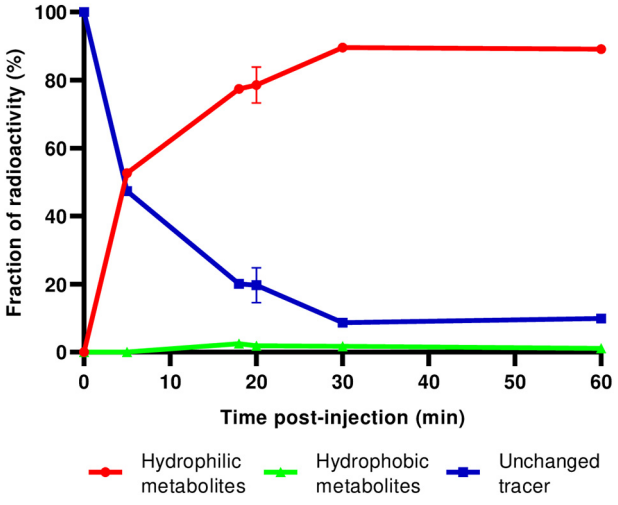

Fig. 4. Proportions of [^{18}F]fluoropyridine-candesartan and its labeled metabolites in rat plasma over time after IV injection. [^{18}F]Fluoropyridine-candesartan is metabolized to give mainly hydrophilic labeled compounds. Results at 20 min post-injection are expressed as mean ± SD (n = 4).

4. Discussion

The development of novel radiotracers for AT_1R quantification would offer the possibility to improve the diagnostic and guide therapy of several renal and heart diseases by PET imaging. The designed molecules should retain or improve the pharmacokinetic, pharmacodynamic and AT_1R-binding properties of the drugs used as the lead compound. Competitive binding assays demonstrated that fluoropyridine-candesartan and fluoropyridine-losartan display similar binding affinities for the AT_1R and slightly lower than their parent compounds (candesartan and losartan, respectively). These results confirmed that the introduction via click chemistry (Huisgen 1,3-dipolar Cu(I)-catalyzed azide–alkyne cycloaddition reaction) of the fluoropyridine moiety on candesartan and losartan did not affect considerably their binding properties. Recently, the AT_1R binding affinity of the ammoniomethyltrifluoroborate derivative of losartan ($AMBF_3$Los, Ki = 7.9 nM) was reported [14]. The structures of the fluoropyridine derivatives and $AMBF_3$Los (Fig. 1) contain a common moiety, the 1,2,3-triazole ring formed from the cycloaddition click reaction. In drug design, triazoles are employed as bioisosteres of amides, esters, and carboxylic acids, and as linkers to increase the efficacy of the lead molecules [37–40]. Triazoles possess a strong dipole moment [41,42], pi electron-

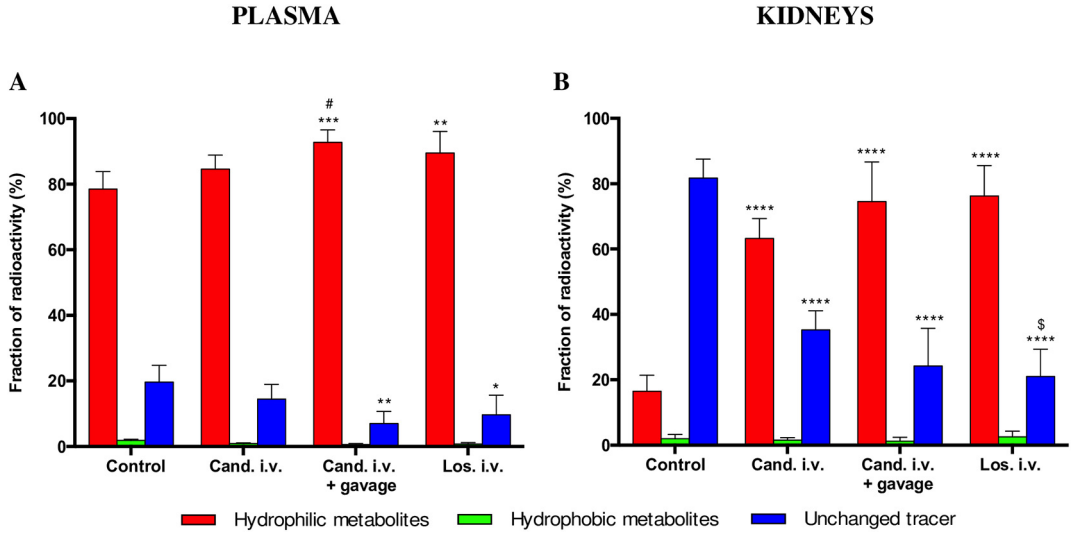

Fig. 5. Proportions of [^{18}F]fluoropyridine-candesartan and its labeled metabolites in (A) control rat's plasma and (B) kidneys at 20 min post-injection, n = 4. Effect of AT_1R blocking with candesartan (IV, 10 mg/kg; IV, 5 mg/kg + gavage, 5 mg/kg) or losartan (IV, 30 mg/kg), n = 4 in each group. Data are presented as mean ± SD. *–**** blocking groups vs control, $^{*}p < 0.05$, $^{**}p < 0.01$, $^{***}p < 0.001$, $^{****}p < 0.0001$; #$p < 0.05$ candesartan IV + gavage group vs candesartan IV; \$$p < 0.05$ losartan IV vs candesartan IV group.

deficient aromaticity, and good hydrogen-bond accepting capacity. These properties could explain the high binding affinity of fluoropyridine-candesartan and fluoropyridine-losartan as a result of strong interactions with the AT_1R binding sites, when the triazole is used as a bioisostere of the carboxylic acid on candesartan. The main metabolite of losartan (EXP3174, Fig. 1) also contains a carboxylic group, which increases its binding affinity (IC_{50} = 0.45 nM) compared to losartan (IC_{50} = 34 nM) [43].

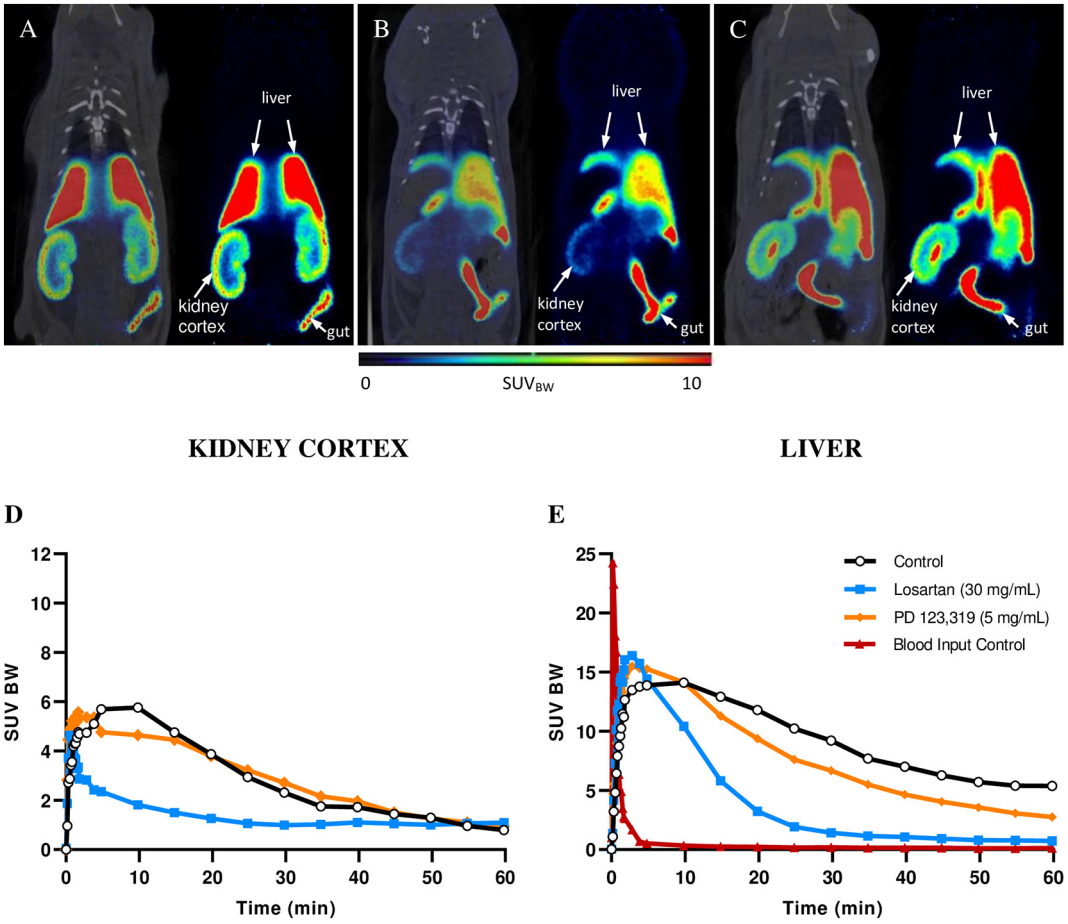

Fig. 6. Representative microPET/CT and PET images (coronal view) of [^{18}F]fluoropyridine-candesartan showing liver and kidney uptakes at 10–20 min post-injection in (A) control, (B) blocked with losartan (30 mg/kg) and (C) treated with PD 123,319 (5 mg/kg) rats. Images are displayed using the same SUV_{BW} scale. Representative tracer time-activity curves for (D) left kidney cortex and (E) liver (superior part of the right lobe) are presented as specific uptake values normalized to body weight (SUV_{BW}) from 0 to 60 min scans.

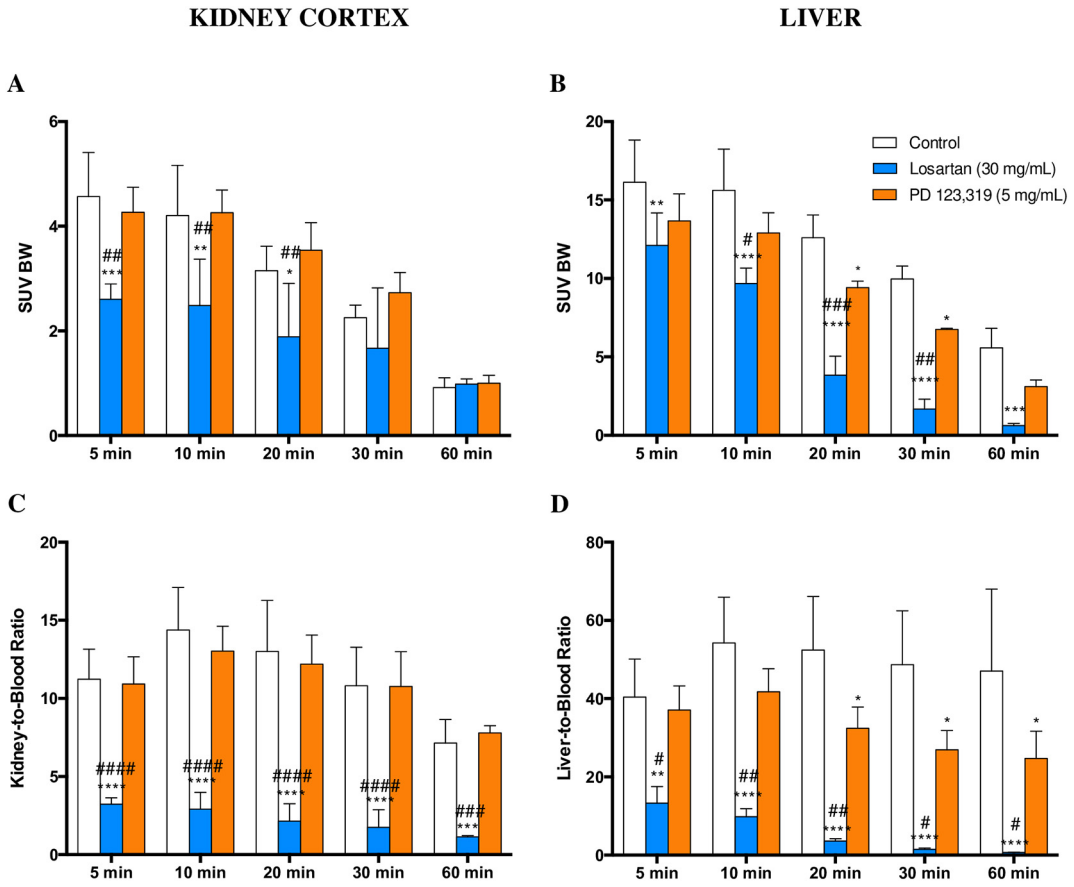

Fig. 7. Comparison of SUV_{BW} and tissue-to-blood ratios of [^{18}F]fluoropyridine-candesartan in control (n = 6) and treated with losartan (30 mg/kg, n = 3) or PD 123,319 (5 mg/kg, n = 3) animals, SUV_{BW} in (A) kidney cortex and (B) liver, tissue-to-blood ratio in (C) kidney cortex and (D) liver. Data are presented as mean ± SD. *–**** losartan and PD 123,319 groups vs control, $^{*}p < 0.05$, $^{**}p < 0.01$, $^{***}p < 0.001$, $^{****}p < 0.0001$; #–#### losartan vs PD 123,319 group, $\#p < 0.05$, $\#\#p < 0.01$, $\#\#\#p < 0.001$, $\#\#\#\#p < 0.0001$.

Conversely, fluorobenzyl-candesartan exhibited the lowest binding affinity among all derivatives, comparable with fluoroethyl-losartan (FEtLos, Ki = 2200 nM) [14]. Both ligands present an ether group bound to a hydrophobic chain (Fig. 1), apparently generating weaker electrostatic interactions with the AT_1R binding sites, and possibly reducing the binding to AT_1R. In addition, the phenyl-alkyne planar arrangement (sp^2-sp carbon-carbon bond) on fluorobenzyl-candesartan could imply an increase in steric hindrance to AT_1R interactions and a reduction in polarity compared to fluoropyridine-candesartan. In fact, fluorobenzyl-candesartan is more hydrophobic (cLogP = 7.7) than fluoropyridine-candesartan (cLogP = 6.1) and candesartan (cLogP = 5), suggesting that replacing the carboxylic group on candesartan by a low-polarity moiety considerably reduces the affinity for the AT_1R.

The AT_1R are expressed in the kidneys, liver, adrenal glands, heart, brain, gut and vascular tissues in numerous species [44,45]. The PET signal reduction of [^{18}F]fluoropyridine-candesartan in the AT_1R-rich renal cortex of rats pre-treated with the AT_1R antagonist losartan confirmed our previous results using ex vivo biodistribution in rats and in vitro binding studies [33]. Administration of saturating doses of the AT_2R antagonist PD 123,319 had no significant effect on tracer uptake (SUV_{BW} or tissue-to-blood ratios) in kidney cortex over time, confirming [^{18}F] fluoropyridine-candesartan binding selectivity for AT_1R over AT_2R at tracer doses.

The reductions of the liver SUV_{BW} and tissue-to-blood ratios in rats pretreated with losartan, suggest specific binding to hepatic AT_1R. As reported in the literature, the AT_1R are also widely expressed in the liver [45,46] and are involved in the development of various hepatic diseases [5,47,48]. However, the long-lasting retention of [^{18}F]fluoropyridine-candesartan in the liver of control animals could also be related to the metabolism of the tracer by the hepatobiliary system as it occurs with most ARB drugs [49]. Candesartan is mostly excreted via the renal route (60%) after IV injection [50]. Nevertheless, the introduction of the [^{18}F] fluoropyridine moiety on candesartan renders the derivative more lipophilic than its parent compound (carboxylic acid), and possibly increases the contribution of the hepatobiliary excretion pathway given the relationship between lipophilicity and hepatic metabolism [51]. This will need to be determined in the future. Interestingly, a ^{11}C-derivative of the AT_1R antagonist telmisartan was tested as a tracer of the hepatic transporters OATP1B3 in rats [52], considering its selective liver uptake and primary hepatobiliary excretion (>98%) [50]. A dose dependent reduction of the tracer uptake was reported in the liver after administration of the OATP inhibitor rifampicin or the AT_1R antagonist telmisartan [52]. On the other hand, administration of the AT_2R antagonist PD 123,319 also reduced the hepatic retention of [^{18}F] fluoropyridine-candesartan after 20 min post-injection compared to control rats. Conversely, several studies demonstrated the absence of AT_2R in the liver [46], hence the observed reduction is likely not related to AT_2R binding. The decrease in liver uptake after pre-treatment with PD 123,319 could be associated to the binding to hepatic transporters [53]. A high liver uptake was also reported for previous AT_1R tracers [15–21,24]. To better understand the nature of the pharmacokinetic processes that take place in the liver, further work will need to be accomplished, such as the assessment of unchanged tracer and the presence of labeled metabolites in rat's liver in normal and blocking conditions, and PET imaging studies in the presence of the OATP inhibitors, such as rifampicin, to evaluate binding to hepatic transporters.

[^{18}F]Fluoropyridine-candesartan demonstrated higher uptake in the renal cortex ($SUV_{BW} = 4.2 \pm 0.9$) compared to [^{18}F]fluoropyridine-losartan ($SUV_{BW} = 1.5 \pm 0.6$) [18] at 10 min post-injection and a slower

clearance. It should be noted that surmountable inhibition, as with losartan, results from fast and reversible binding of the antagonist to the receptor, whereas insurmountable inhibition, as with candesartan, is related to a slower dissociation of the receptor-antagonist complex [32,43,54]. Therefore, the longer retention observed with [^{18}F]fluoropyridine-candesartan in the kidney cortex was anticipated due to the longer dissociation time of candesartan (66 min) from the binding sites in the AT_1R compared to losartan (2.5 min) [54].

The presence of 82% of unmetabolized [^{18}F]fluoropyridine-candesartan in kidneys (higher fraction than [^{11}C]methyl-candesartan (<70%) [21] at 20 min post-injection and slow metabolism (42% at 60 min post-injection) confirms the favorable pharmacokinetics of the tracer with regards to measuring AT_1R. Pre-treatment with AT_1R antagonists reduced the unchanged [^{18}F]fluoropyridine-candesartan proportion in rat's kidneys, indicating blockade of AT_1R binding sites and thus, tracer specificity. The main products of [^{18}F]fluoropyridine-candesartan metabolism, i.e. hydrophilic labeled metabolites, are associated with non-specific binding as they were not blocked by AT_1R antagonists. Furthermore, the novel tracer overcomes the limitations of [^{11}C]methyl-candesartan regarding the interference of its hydrophobic labeled metabolite, the desethyl derivative [^{11}C]TH4 (Fig. 1), in PET imaging [21], as the proportion in kidneys of the hydrophobic labeled metabolites generated from [^{18}F]fluoropyridine-candesartan (in negligible amounts) was not reduced after blockage. It is important to note that the whole kidneys were processed for metabolism studies, thus the distribution of unchanged tracer and metabolites in specific areas such as the kidney cortex was not analyzed.

Additionally, [^{18}F]fluoropyridine-candesartan also offers the advantages inherent to fluorine-18 radionuclide over carbon-11 ([^{11}C]methyl-candesartan), such as a longer half-life (110 min vs. 20 min) which allows for multiple scans per tracer formulation, shipment to other imaging facilities, and longer imaging protocols including exhaustive metabolism studies; and lower positron energy (0.64 MeV vs. 0.96 MeV) providing shorter linear range in live tissues, thus higher resolution PET images [55].

[^{18}F]Fluoropyridine-candesartan binding to plasma proteins (99.3%) is in agreement with the pharmacological characteristics of its parent compound candesartan (99.5%) [50] and the analogue [^{11}C]methyl-candesartan (99.8%) [21]. Similar results were reported for other ARBs (e.g. losartan (98.7%), valsartan (95%), telmisartan (>98%)) [50] and the radiolabeled derivative [^{18}F]fluoropyridine-losartan (97%) [18]. Despite the high levels of protein binding, these agents achieve pharmacologically significant concentrations at the AT_1R, as evidenced by their ability to antagonize Ang II mediated effects [18,50]. According to our study, less than 1% of [^{18}F]fluoropyridine-candesartan was available to interact with the AT_1R in rat tissues, nevertheless providing excellent PET images.

The results presented here suggest a high potential of [^{18}F]fluoropyridine-candesartan for PET quantification of renal AT_1R, since the signal corresponding to specific binding to these receptors is mainly generated from the parent tracer and not from hydrophilic labeled metabolites detected in the kidneys, contrary to [^{11}C]methyl-candesartan. Furthermore, our findings revealed that [^{18}F]fluoropyridine-candesartan exhibits higher signal-to-noise ratios and longer retention than [^{18}F]fluoropyridine-losartan in rat kidney cortex, offering a new modality of PET imaging of AT_1R with greater resolution and sensitivity.

5. Conclusions

High kidney-to-blood ratios and binding selectivity to renal AT_1R over AT_2R combined with high in vivo stability producing minimal interference from labeled hydrophobic metabolites on the PET signal support further PET imaging with [^{18}F]fluoropyridine-candesartan. This novel high-affinity derivative of the clinically-used ARB candesartan has a good potential for PET quantification of AT_1R.

Declaration of competing interest

The authors declare that they have no known competing financial interests or personal relationships that could have appeared to influence the work reported in this paper.

Acknowledgements

This work was supported by the Canadian Institutes of Health Research (MOP-126079) and was conducted as part of the TransMedTech Institute's activities and thanks, in part, to funding from Fonds de recherche du Québec. The authors thank the staffs of the Radiochemistry & Cyclotron platform (CRCHUM) and the Small Animal Imaging Labs (MUHC Research Institute) for their assistance in the radiosyntheses and PET/CT scans, respectively.

References

[1] Nehme A, Zouein FA, Deris Zayeri Z, Zibara K. An update on the tissue renin angiotensin system and its role in physiology and pathology, vol. 6; 2019; 14.
[2] Paul M, Mehr AP, Kreutz R. Physiology of local renin-angiotensin systems, vol. 86; 2006; 747–803.
[3] Zhu Y, Cui H, Lv J, Liang H, Zheng Y, Wang S, et al. AT1 and AT2 receptors modulate renal tubular cell necroptosis in angiotensin II-infused renal injury mice. Sci Rep. 2019;9:19450.
[4] Unger T. The role of the renin-angiotensin system in the development of cardiovascular disease. Am J Cardiol. 2002;89:3–9.
[5] Shim KY, Eom YW, Kim MY, Kang SH, Baik SK. Role of the renin-angiotensin system in hepatic fibrosis and portal hypertension. Korean J Intern Med. 2018;33:453–61.
[6] Suganuma T, Ino K, Shibata K, Kajiyama H, Nagasaka T, Mizutani S, et al. Functional expression of the angiotensin II type1 receptor in human ovarian carcinoma cells and its blockade therapy resulting in suppression of tumor invasion, angiogenesis, and peritoneal dissemination. . 2005;11:2686–94.
[7] Xu ZG, Lanting L, Vaziri ND, Li Z, Sepassi L, Rodriguez-Iturbe B, et al. Upregulation of angiotensin II type 1 receptor, inflammatory mediators, and enzymes of arachidonate metabolism in obese Zucker rat kidney: reversal by angiotensin II type 1 receptor blockade. Circulation. 2005;111:1962–9.
[8] Jazmín F-M, Diego L-M, Luisa M-A. Function of renin angiotensin system on heart failure. J Integr Cardiol. 2016;2.
[9] Evangelista Fs FP. Complications of type 1 diabetes mellitus are associated with renin angiotensin system: the role of physical exercise as therapeutic tool. Pancr Disord Ther. 2014;04.
[10] Muneer K, Nair A. Angiotensin-converting enzyme inhibitors and receptor blockers in heart failure and chronic kidney disease — demystifying controversies. Indian Heart J. 2017;69:371–4.
[11] Fonarow GC, Yancy CW, Hernandez AF, Peterson ED, Spertus JA, Heidenreich PA. Potential impact of optimal implementation of evidence-based heart failure therapies on mortality. Am Heart J. 2011;161:1024–30 [e3].
[12] Pfeffer MA, Swedberg K, Granger CB, Held P, McMurray JJV, Michelson EL, et al. Effects of candesartan on mortality and morbidity in patients with chronic heart failure: the CHARM-Overall programme. Lancet. 2003;362:759–66.
[13] Tsoi B, Akioyamen LE, Bonner A, Frankfurter C, Levine M, Pullenayegum E, et al. Comparative efficacy of angiotensin II antagonists in essential hypertension: systematic review and network meta-analysis of randomised controlled trials. Heart Lung Circ. 2018;27:666–82.
[14] Sahylí Ortega Pijeira M, Sérgio Gonçalves Nunes P, Nascimento dos Santos S, Zhang Z, Pérez Nario A, Araujo Perini E, et al. Synthesis and evaluation of [^{18}F]FEtLos and [^{18}F]AMBF3Los as novel ^{18}F-labelled losartan derivatives for molecular imaging of angiotensin II type 1 receptors. Molecules. 2020;25:1872.
[15] Hoffmann M, Chen X, Hirano M, Arimitsu K, Kimura H, Higuchi T, et al. ^{18}F-labeled derivatives of Irbesartan for angiotensin II receptor PET imaging. ChemMedChem. 2018;13:2546–57.
[16] Chen X, Hirano M, Werner RA, Decker M, Higuchi T. Novel ^{18}F-labeled PET imaging agent FV45 targeting the renin-angiotensin system. ACS Omega. 2018;3:10460–70.
[17] Arksey N, Hadizad T, Ismail B, Hachem M, Valdivia AC, Beanlands RS, et al. Synthesis and evaluation of the novel 2-[^{18}F]fluoro-3-propoxy-triazole-pyridine-substituted losartan for imaging AT_1 receptors. Bioorg Med Chem. 2014;22:3931–7.
[18] Hachem M, Tiberi M, Ismail B, Hunter CR, Arksey N, Hadizad T, et al. Characterization of ^{18}F-FPyKYNE-losartan for imaging AT1 receptors. J Nucl Med. 2016;57:1612–7.
[19] Ismail B, Hadizad T, Antoun R, Lortie M, deKemp RA, Beanlands RSB, et al. Evaluation of [^{11}C]methyl-losartan and [^{11}C]methyl-EXP3174 for PET imaging of renal AT1 receptor in rats. Nucl Med Biol. 2015;42:850–7.
[20] Hadizad T, Kirkpatrick SA, Mason S, Burns K, Beanlands RS, DaSilva JN. Novel O-[^{11}C]methylated derivatives of candesartan as angiotensin II AT_1 receptor imaging ligands: radiosynthesis and ex vivo evaluation in rats. Bioorg Med Chem. 2009;17:7971–7.
[21] Lortie M, DaSilva JN, Kirkpatrick SA, Hadizad T, Ismail BA, Beanlands RS, et al. Analysis of [^{11}C]methyl-candesartan kinetics in the rat kidney for the assessment of angiotensin II type 1 receptor density in vivo with PET. Nucl Med Biol. 2013;40:252–61.
[22] Ismail B, deKemp RA, Croteau E, Hadizad T, Burns KD, Beanlands RS, et al. Treatment with enalapril and not diltiazem ameliorated progression of chronic kidney disease

in rats, and normalized renal AT1 receptor expression as measured with PET imaging. PLoS One. 2017;12:e0177451.
[23] Ismail B, deKemp RA, Hadizad T, Mackasey K, Beanlands RS, DaSilva JN. Decreased renal AT1 receptor binding in rats after subtotal nephrectomy: PET study with [^{18}F]FPyKYNE-losartan. EJNMMI Res. 2016;6:55.
[24] Zober TG, Mathews WB, Seckin E, Yoo S-E, Hilton J, Xia J, et al. PET imaging of the AT1 receptor with [^{11}C]KR31173. Nucl Med Biol. 2006;33:5–13.
[25] Xia J, Seckin E, Xiang Y, Vranesic M, Mathews WB, Hong K, et al. Positron-emission tomography imaging of the angiotensin II subtype 1 receptor in swine renal artery stenosis. Hypertension. 2008;51:466–73.
[26] Gulaldi N, Xia J, Feng T, Hong K, Mathews W, Ruben D, et al. Modeling of the renal kinetics of the AT1 receptor specific PET radioligand [^{11}C]KR31173. Biomed Res Int. 2013;2013:835859.
[27] Higuchi T, Fukushima K, Xia J, Mathews WB, Lautamaki R, Bravo PE, et al. Radionuclide imaging of angiotensin II type 1 receptor upregulation after myocardial ischemia-reperfusion injury. J Nucl Med. 2010;51:1956–61.
[28] Fukushima K, Bravo PE, Higuchi T, Schuleri KH, Lin X, Abraham MR, et al. Molecular hybrid positron emission tomography/computed tomography imaging of cardiac angiotensin II type 1 receptors. J Am Coll Cardiol. 2012;60:2527–34.
[29] Valenta I, Szabo Z, Mathews WB, Abraham TP, Abraham MR, Schindler TH. PET/CT imaging of cardiac angiotensin II type 1 receptors in nonobstructive hypertrophic cardiomyopathy. JACC Cardiovasc Imaging. 2019;12:1895–6.
[30] Fuchs B, Breithaupt-Grögler K, Belz GG, Roll S, Malerczyk C, Herrmann V, et al. Comparative pharmacodynamics and pharmacokinetics of candesartan and losartan in man. J Pharm Pharmacol. 2000;52:1075–83.
[31] van Rodijnen WF, van Lambalgen TA, van Teijlingen ME, Tangelder G-J, ter Wee PM. Comparison of the AT1-receptor blockers candesartan, irbesartan and losartan for inhibiting renal microvascular constriction. J Renin Angiotensin Aldosterone Syst. 2001;2:S204–10.
[32] Vauquelin G, Fierens F, Liefde I. Long-lasting angiotensin type 1 receptor binding and protection by candesartan: comparison with other biphenyl-tetrazole sartans. J Hypertens Suppl. 2006;24:S23–30.
[33] Abreu Diaz AM, Drumeva GO, Petrenyov DR, Carrier J-F, DaSilva JN. Synthesis of the novel AT1 receptor tracer [^{18}F]fluoropyridine–candesartan via click chemistry. ACS Omega. 2020;5:20353–62.
[34] Alonso Martinez LM, DaSilva JN. Development of a novel [^{18}F]fluorobenzyl derivative of the AT1 receptor antagonist Candesartan. J Label Compd Radiopharm. 2020:1–9.
[35] Kenk M, Greene M, Lortie M, deKemp RA, Beanlands RS, DaSilva JN. Use of a column-switching high-performance liquid chromatography method to assess the presence of specific binding of (R)- and (S)-[^{11}C]rolipram and their labeled metabolites to the phosphodiesterase-4 enzyme in rat plasma and tissues. Nucl Med Biol. 2008;35:515–21.
[36] Dornan MH, Petrenyov D, Simard J-M, Aliaga A, Xiong G, Ghislain J, et al. A high molar activity ^{18}F-labeled TAK-875 derivative for PET imaging of pancreatic β-cells. EJNMMI Radiopharm Chem. 2018;3:14.
[37] Bonandi E, Christodoulou MS, Fumagalli G, Perdicchia D, Rastelli G, Passarella D. The 1,2,3-triazole ring as a bioisostere in medicinal chemistry. Drug Discov Today. 2017;22:1572–81.
[38] Giraudo A, Krall J, Nielsen B, Sorensen TE, Kongstad KT, Rolando B, et al. 4-Hydroxy-1,2,3-triazole moiety as bioisostere of the carboxylic acid function: a novel scaffold to probe the orthosteric gamma-aminobutyric acid receptor binding site. Eur J Med Chem. 2018;158:311–21.
[39] Malik MS, Ahmed SA, Althagafi II, Ansari MA, Kamal A. Application of triazoles as bioisosteres and linkers in the development of microtubule targeting agents. RSC Med Chem. 2020;11:327–48.
[40] Song WH, Liu MM, Zhong DW, Zhu YL, Bosscher M, Zhou L, et al. Tetrazole and triazole as bioisosteres of carboxylic acid: discovery of diketo tetrazoles and diketo triazoles as anti-HCV agents. Bioorg Med Chem Lett. 2013;23:4528–31.
[41] Joshi S, Bhattacharjee R, Sarmah DA, Sakhuja R, Pant D, Joshi S, et al. Experimental and theoretical study: determination of dipole moment of synthesized coumarin–triazole derivatives and application as turn off fluorescence sensor: high sensitivity for iron(III) ions. Sens Actuators B. 2015;220.
[42] Rodios NA, Alexandrou NE. Dipole moments. Structure and conformation of asymmetrically 4,5-substituted 1-(α-aroyloxyarylideneamino)-1,2,3-triazoles, vol. 16; 1979; 571–5.
[43] Vanderheyden PM, Fierens FL, De Backer JP, Fraeyman N, Vauquelin G. Distinction between surmountable and insurmountable selective AT1 receptor antagonists by use of CHO-K1 cells expressing human angiotensin II AT1 receptors. Br J Pharmacol. 1999;126:1057–65.
[44] Allen AM, Zhuo J, Mendelsohn FAO. Localization and function of angiotensin AT1 receptors. Am J Hypertens. 2000;13:31S–8S.
[45] de Gasparo M, Catt KJ, Inagami T, Wright JW, Unger T. International union of pharmacology. XXIII. The angiotensin II receptors. Pharmacol Rev. 2000;52:415–72.
[46] Miyata N, Park F, Li XF, Cowley Jr AW. Distribution of angiotensin AT1 and AT2 receptor subtypes in the rat kidney. Am J Physiol. 1999;277:F437–46.
[47] Fan F, Tian C, Tao L, Wu H, Liu Z, Shen C, et al. Candesartan attenuates angiogenesis in hepatocellular carcinoma via downregulating AT1R/VEGF pathway. Biomed Pharmacother. 2016;83:704–11.
[48] Abd El-Rahman SS, Fayed HM. Targeting AngII/AT1R signaling pathway by perindopril inhibits ongoing liver fibrosis in rat. J Tissue Eng Regen Med. 2019;13:2131–41.
[49] Israili ZH. Clinical pharmacokinetics of angiotensin II (AT1) receptor blockers in hypertension. J Hum Hypertens. 2000;14:S73–86.
[50] Oparil S. Newly emerging pharmacologic differences in angiotensin II receptor blockers. Am J Hypertens. 2000;13:18S–24S.
[51] McEuen K, Borlak J, Tong W, Chen M. Associations of drug lipophilicity and extent of metabolism with drug-induced liver injury. Int J Mol Sci. 2017;18.
[52] Takashima T, Hashizume Y, Katayama Y, Murai M, Wada Y, Maeda K, et al. The involvement of organic anion transporting polypeptide in the hepatic uptake of telmisartan in rats: PET studies with [^{11}C]telmisartan. Mol Pharm. 2011;8:1789–98.
[53] Testa A, Zanda M, Elmore CS, Sharma P. PET tracers to study clinically relevant hepatic transporters. Mol Pharm. 2015;12:2203–16.
[54] Ojima M, Inada Y, Shibouta Y, Wada T, Sanada T, Kubo K, et al. Candesartan (CV-11974) dissociates slowly from the angiotensin AT1 receptor. Eur J Pharmacol. 1997;319:137–46.
[55] Boschi S, Lodi F. Chemistry of PET radiopharmaceuticals: labelling strategies. In: Khalil MM, editor. Basic science of PET imaging. Cham: Springer International Publishing; 2017. p. 79–103.